a reprint from Applied Optics

Aberration-corrected concave grating for the mid-infrared spectrometer aboard the Infrared Telescope in Space

Takashi Onaka

A mechanically ruled aberration-corrected concave grating was developed for use in the low-resolution mid-infrared spectrometer aboard the cryogenically cooled Infrared Telescope in Space. The design and the performance testing of the grating are reported. The spectrometer requires a wide spectral range (4.5–11.7 μm) and a wide field of view (8 × 8 arcmin) with a low wavelength resolution ($\Delta\lambda \leq 0.3$ μm). The aberration-corrected concave grating provides a flat focal plane with a small aberration in the spatial direction compared with those caused by the finite size of the entrance slit. It also permits a simple design for the spectrometer, which is advantageous for applications in space cryogenic instruments. The measurements of the wavelength resolution and the spatial resolution are shown to be in good agreement with the predicted performance. The diffraction efficiency of the grating is more than 80% at the blaze wavelength (6 μm) and fairly high (> 30%) over the entire wavelength range in question. The grating produces polarization of less than 10% for $\lambda < 6.4$ μm and of 10–20% for 6.7 μm $< \lambda <$ 9.7 μm. These results indicate the potential applicability of this type of grating to the wide-field IR spectroscopic observations.

Key words: Concave grating, infrared spectrometer, space instrument.

1. Introduction

The mid-infrared spectrometer (MIRS) is a low-resolution ($\lambda/\Delta\lambda \sim 15$–30), wide-field-of-view (8 × 8 arcmin) spectrometer intended to cover a wide mid-IR spectral range (4.5–11.7 μm); it is aboard the Infrared Telescope in Space (IRTS) to be launched in early 1995. Details of the MIRS design and the IRTS mission are described in other references.[1,2] The objective of the MIRS is to take mid-IR spectra of both extended and point sources, taking advantage of the wide-field-of-view characteristics of the IRTS.[3] This is in contrast to the low-resolution spectrometer[4] aboard the Infrared Astronomical Satellite, which was of a slitless design and could be effective only in the observation of point sources. The MIRS has a wide field of view compared with ISOPHOT-S,[5] a low-resolution spectrometer aboard the Infrared Space Observatory, and thus it is efficient in the observation of diffuse sources. Because the thermal zodiacal emission dominates the background radiation in the mid-IR region, it is important for the spectrometer to have a well-defined spatial resolution to reduce the background contamination in wide-field-of-view observations. A good beam pattern for the wide field of view requires a fast camera with low aberration in the conventional spectrometer design, which may be realized by sophisticated optics. However, a space instrument has strict restrictions on the weight and size. In addition, IR instruments have to work at cryogenic temperatures (below 2 K for the MIRS) to suppress the thermal background radiation. Therefore it is desirable to have a simple design that enables ease of assembly and alignment.

One way to meet these requirements is to adopt a standard spectrometer design consisting of a collimator and a camera incorporating sophisticated optics to decrease the size and aberrations. This is the design adopted in the near-infrared spectrometer (NIRS), which is also to be aboard the IRTS.[6] The MIRS, on the other hand, takes another design approach, in which an aberration-corrected concave grating is used. The use of the concave grating permits the elimination of collimator and camera mirrors and thus enables a quite simple design.[1] The mechanically ruled aberration-corrected grating has a further advantage in that it can reduce astigmatic aberrations otherwise inherent in classical concave gratings.[7]

The author is with the Department of Astronomy, School of Science, University of Tokyo, Bunkyo-ku, Tokyo 113, Japan.

Received 20 April 1994; revised manuscript received 5 July 1994.
0003 6935/95/040650 08$06.00/0.

The aberration-corrected type of grating has been developed mainly for the UV–visual applications, where a small number of reflection surfaces is essential to obtain a high efficiency. The benefit of mechanically ruled aberration-corrected gratings in the visual–UV range has been demonstrated in several applications, and the production technology has been well established.[8]

However, the application of such a grating to the MIRS necessitates that some new features be investigated, such as relatively deep grooves required for IR use, a relatively deep curvature to match the fast beam from the incident light of the IRTS ($f/4$, 15-cm primary mirror), and a wide spectral range. The use at low temperature is also an additional requirement, but it is not investigated in here. In this paper I describe the design of the MIRS grating and report the results of the performance testing of the flight model of the grating at room temperature, including the wavelength resolution, the spatial resolution, the diffraction efficiency, and the polarization characteristics. The grating at the low operating temperature of the MIRS showed no serious degradation in its performance when tested after integration onto the spectrometer.[1]

2. Design of the MIRS Grating

2.A. Basic Equations of an Aberration-Corrected Concave Grating with a Finite Slit Length

A general description of the characteristics of aberration-corrected concave gratings is given by Harada and Kita.[8] The design of the MIRS grating is briefly summarized here.

The Cartesian coordinate system is shown in Fig. 1, where origin O is at the center of the grating surface. The light coming through point $A(x, y, z)$, falling on point $P(u, w, l)$ on the grating surface, and diffracted to point $B(x', y', z')$ is considered. Note that the current description includes the finite slit length ($z \neq 0$), which is neglected in Ref. 8.

The light path function F, A through P to B, is defined as

$$F = \langle AP \rangle + \langle PB \rangle + mn\lambda, \qquad (1)$$

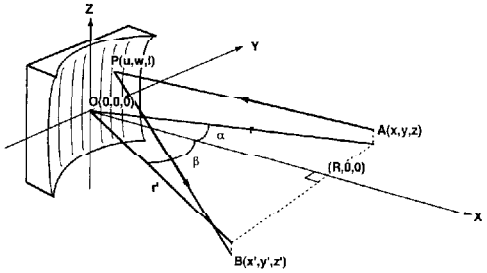

Fig. 1. Schematic diagram of the coordinate system.

where m is the order of diffraction, λ is the wavelength of the light, and n is the groove number at P defined below. For the application to the MIRS, A and B are taken to be on the plane that includes the center of curvature of the grating and is perpendicular to the grating (Fig. 1) or

$$r = R/\cos\alpha, \qquad r' = R/\cos\beta, \qquad (2)$$

where R is the radius of the curvature of the grating, α and β are the angles of incidence and diffraction, respectively, and r and r' are the distances from the center of the grating to the projected points of A and B on the X Y plane, respectively. This choice defines a flat focal plane, which is advantageous in applications to instruments with solid detector arrays. Because A and B are taken on the plane including the center of curvature of the grating, the aberrations in the vertical direction (Z) are minimized because of the nature of the spherical surface. With constant-spacing grooves (classical concave grating) the horizontal focal curve is given by the Rowland circle and is not a flat plane. It does not agree with the vertical focal curve either (see Fig. 2). Variable-spacing grooves can approximately adjust both the horizontal and vertical focal curves to the flat plane and reduce the aberration significantly.

The tilt angle of the groove (denoted as θ in Ref. 8), which can be used to adjust the linearity of wavelength with position on the focal plane, is set at zero in the MIRS grating design, because a fairly good linearity is predicted even with $\theta = 0$ (see Fig. 7) and because this eliminates most aberrations in the slit

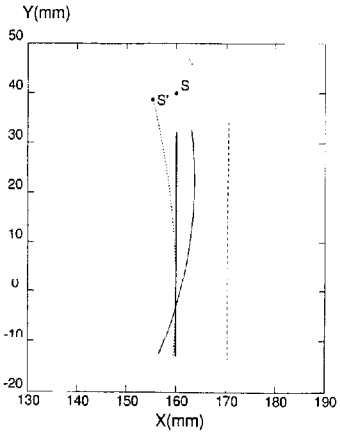

Fig. 2. Locations of the focal curves on the X–Y plane. The thin solid curve and thick solid line indicate the horizontal and vertical focal curves for the MIRS grating, respectively. The detector positions agree exactly with the vertical focal curve (the thick straight line). The slit position is indicated by S. For comparison, the Rowland circle and the vertical focal curve corresponding to the slit position with the same incident angle S' are plotted by the dotted curve and dashed line, respectively.

direction. In the following equations, the parameter θ is thus omitted.

The groove number n is a variable dependent on the grating position and is defined as

$$n = \left(w + \frac{b_2}{R} w^2 + \frac{b_3}{R^2} w^3 + \frac{b_4}{R^3} w^4 + \cdots\right) \Big/ \sigma_0, \quad (3)$$

where σ_0 is the groove spacing at $w=0$ and b_i is the ruling parameter. In the MIRS grating design, terms of orders higher than b_4 are neglected.

With these conditions, the light path function can be given by a power series of w and l as

$$F = r + r' + \frac{z^2}{2r} + \frac{z'^2}{2r'} + wF_{10} + w^2F_{20} + w^3F_{30} + w^4F_{40} + \cdots + lG_{01} + wlG_{11} + wG_{10} + \cdots. \quad (4)$$

The terms containing l without z in the original formulation[8] become zero owing to the conditions of Eq. (2). The terms containing G come from the finite length of the entrance slit. Only aberrations resulting from the finite slit length remain in the spatial direction.

The factors F_{10}, F_{20}, F_{30}, and F_{40} are functions of r and r' only and are given, in the conditions of Eq. (2), by

$$F_{10} = -(\sin\alpha + \sin\beta) + \frac{m\lambda}{\sigma_0}, \quad (5)$$

$$F_{20} = -\frac{1}{2R}(\cos\alpha \sin^2\alpha + \cos\beta \sin^2\beta) + \frac{m\lambda}{\sigma_0}\frac{b_2}{R}, \quad (6)$$

$$F_{30} = -\frac{1}{2R^2}(\cos^2\alpha \sin^3\alpha + \cos^2\beta \sin^3\beta) + \frac{m\lambda}{\sigma_0}\frac{b_3}{R^2}, \quad (7)$$

$$F_{40} = -\frac{5}{8R^3}(\cos^3\alpha \sin^4\alpha + \cos^3\beta \sin^4\beta) + \frac{m\lambda}{\sigma_0}\frac{b_4}{R^3}. \quad (8)$$

The factors G_{01}, G_{11}, and G_{10} are given by

$$G_{01} = -\left(\frac{z}{r} + \frac{z'}{r'}\right), \quad (9)$$

$$G_{11} = -\left(\frac{z}{r^2}\sin\alpha + \frac{z'}{r'^2}\sin\beta\right), \quad (10)$$

$$G_{10} = \frac{1}{2}\left[\left(\frac{z}{r}\right)^2 \sin\alpha + \left(\frac{z'}{r'}\right)^2 \sin\beta\right]. \quad (11)$$

Fermat's principle

$$\partial F/\partial w = \partial F/\partial l = 0 \quad (12)$$

leads to the well-known grating equation from the F_{10} term as

$$\frac{m\lambda}{\sigma_0} = \sin\alpha + \sin\beta. \quad (13)$$

Equation (13) can be satisfied for a given wavelength for $z = 0$, but for a finite range of wavelengths, Eq. (13) can be satisfied only in an approximate manner and aberration remains. The half-width of the spectral resolution $\Delta\lambda_g$ caused by the aberration for $z = z' = 0$ may be given by

$$\Delta\lambda_g = \frac{1}{2}\frac{\sigma_0}{m}\cos\beta\left|\frac{\partial F}{\partial w}(z = 0; w = W)\right|, \quad (14)$$

where W is the size of the grating in the dispersion direction and $\cos\beta$ takes care of the dependence of β on λ in the grating equation [Eq. (13)]. The ruling parameters b_2, b_3, and b_4 are determined so as to minimize $\Delta\lambda_g$ in the wavelength range in question.

The terms with G factors in Eq. (4) describe the effects of the finite length of the entrance slit. Fermat's principle for the G_{01} term leads to the vertical focus condition,

$$\frac{z}{r} + \frac{z'}{r'} = 0, \quad (15)$$

which indicates the change of the length of the slit image with the position on the focal plane. With the condition of Eq. (15), the maximum deviation Δ in the slit direction resulting from the term G_{11} is given by

$$\Delta = \frac{dW}{4R}\left|\frac{\sin(\alpha - \beta)\cos\alpha}{\cos\beta}\right|, \quad (16)$$

where d is the slit length.

The aberration resulting from G_{10} is called the enveloping curvature of the spectral line.[9] The half-width of the wavelength resolution caused by the aberration in the dispersion direction from G_{11} and G_{10} can be estimated in a manner similar to Eq. (14) as

$$\Delta\lambda_c = \frac{\sigma_0 d\cos\alpha\cos\beta}{8mR^2} \times |[2W\sin(\alpha - \beta) - d\cos\alpha(\sin\alpha + \sin\beta)]|. \quad (17)$$

In the actual design, Δ should be much smaller than the slit length, and $\Delta\lambda_g$ and $\Delta\lambda_c$ should be smaller than the spectral resolution limited by the finite width of the entrance slit or that of the detector. In practice in the MIRS the size of the field mirrors in front of each detector was set to be the same as the slit width, also given by d, and the spectral resolution given by the finite size of the field mirror is therefore

estimated to be

$$\Delta\lambda = \frac{\sigma_0 d}{m R}\cos^3\beta. \tag{18}$$

This gives a good measure of the wavelength resolution resulting from the finite width of the entrance slit and that resulting from the detector size.

If $\Delta\lambda > \Delta\lambda_g, \Delta\lambda_c$, then the full width at half-maximum (FWHM) of the spectral line should be given by $\Delta\lambda$ alone, whereas the full extent of the spectral linewidth will be a summation of all the terms.

2.B. Parameters of the MIRS Grating

The adopted parameters of the MIRS grating are given in Table 1. The wavelength range was determined from the scientific objectives.[1] The space allotted to the MIRS on the focal plane of the IRTS fixed R as 160 mm.[2,3] The grating was sized to collect the entire $f/4$ incident beam. The groove spacing at center σ_0 was fixed by the range of wavelength in use and the detector size for use of the first order, $m = 1$. The astigmatism becomes smaller as the incident angle becomes smaller. In the current grating mount design, however, the entrance slit is located near the longest wavelength point and there must be enough space left for the slit unit and the detector mount. This requirement fixed α as 14°. Given σ_0 and α, the range of β was determined by Eq. (5). The groove parameters b_2, b_3, and b_4 were then chosen to minimize $\Delta\lambda_g$ throughout the given wavelength range.

Figure 2 shows the locations of the vertical ($F_{02} = 0$, thick solid line) and horizontal ($F_{20} = 0$, thin solid curve) focal curves on the X–Y plane. The vertical focal curve is in fact a straight line and agrees exactly with the detector positions. In Fig. 2, the Rowland circle and the vertical focal curve corresponding to the entrance slit on the circle with the same incident angle (=14°) S′ are also plotted by a dotted curve and dashed line, respectively. The variable groove spacings adjust the horizontal and vertical focal curves to the detector position and thus largely reduce the astigmatism.

The MIRS has a wide entrance slit (8 × 8 arcmin or 1.4 mm × 1.4 mm) and covers a wide spectral range with 32 detectors. The spectral resolution limited by the detector field mirror size $\Delta\lambda$ is approximately 0.23 μm. Figure 3 shows the half-width of the spectral line resulting from the detector size $\Delta\lambda$ and that by the grating $\Delta\lambda_g$ according to the adopted parameters. It is clearly indicated that in the current design the grating aberration is small compared with $\Delta\lambda$. The aberration from the finite slit length given by $\Delta\lambda_c$ is negligibly smaller than either of these widths ($< 5 \times 10^{-3}$ μm). The reduction of the slit image size given by Eq. (12) is also small (~3%) and the maximum deviation resulting from the finite slit length Δ never exceeds 0.03 mm. Thus the effects of the finite slit length are essentially negligible in the MIRS design. With these conditions $\Delta\lambda$ can be compared with the measured FWHM of the spectral lines.

These results are confirmed by ray-tracing calculations. Figure 4 depicts the results of ray tracing for all 32 detector positions. Each square corresponds to an element of the field mirror of the detector array, and the corresponding wavelength is indicated below each square. In the calculation, the isotropic light rays of the $f/4$ beam passing through the four corners

Table 1. MIRS Grating Parameters

Wavelength range in use	4.3–11.6 μm
Radius of curvature R	160 mm
Order of diffraction used m	1
Angle of incidence α	14.0°
Angle of diffraction β	−4.6° to +11.27°
Size	49 mm × 49 mm
Effective area	46 mm in diameter
Material	Aluminum alloy 5086
Coating	Gold
Detector[a] and entrance slit size d	1.4 mm × 1.4 mm
Blaze wavelength	6 μm
Diffraction efficiency	> 30% for the entire wavelength range
Ruling parameters	
Groove spacing at center σ_0	26.62 μm
b_2	0.12822
b_3	0.026531
b_4	0.0076869

[a] In the MIRS design the field mirrors were positioned in front of each detector on the focal plane and the real detector size was smaller.

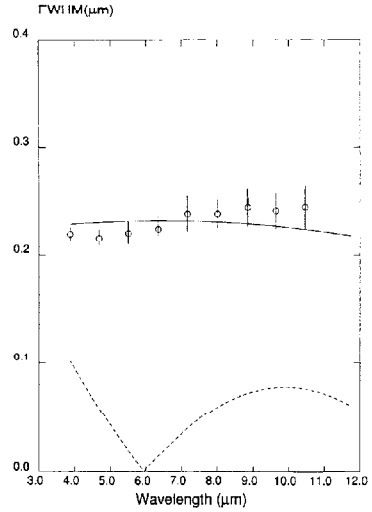

Fig. 3. Spectral line half-width versus wavelength. The solid curve indicates the width resulting from the finite size of the detector $\Delta\lambda$ [Eq. (18)] and the dashed curve shows the width resulting from the grating aberration $\Delta\lambda_g$ [Eq. (14)]. The measured FWHM is plotted by open circles.

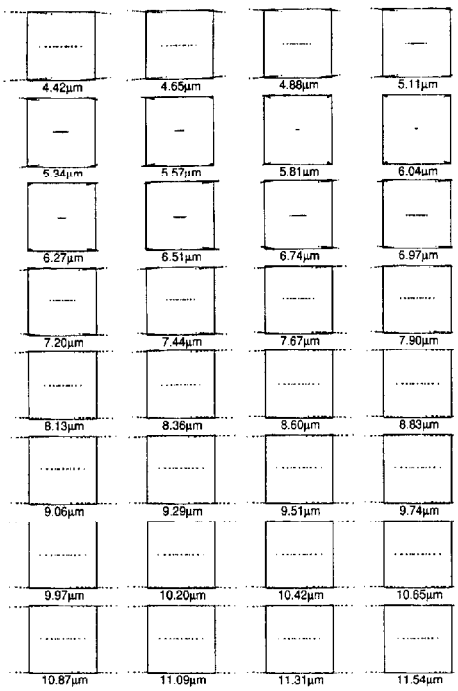

Fig. 4. Results of ray-tracing calculations. Each square expresses the MIRS detectors. The number indicated below the square shows the wavelength of each incident light. For each wavelength, the light rays passing through the four corners and the center of the entrance slit are calculated.

and the center of the entrance slit were traced. The results indicate that the rays through the center always fall within the corresponding square and the aberration is less than the detector size. The performance of the grating shown in Fig. 3 is well demonstrated by the ray-tracing calculation.

The blaze wavelength was set at 6 μm ($\beta \sim 0$). In mechanically ruled concave gratings, the groove angle is usually fixed relative to the Y–Z plane, which leads to a change in the blaze wavelength with the grating position. For the MIRS grating, the surface area was divided into three portions in the Y direction and the groove angles were set to give the same blaze wavelength at the center of each portion to obtain a high efficiency around the blaze wavelength.

The flight grating is a replica of an aluminum alloy 5086 substrate with a gold coating. The grating itself has a stand with two holes for screws to fix the grating to the mount directly. The bottom surface of the stand is used as a reference surface. This enables easy alignment of the grating. The machining errors of the blank were less than 0.2 mm in dimension and less than 3 arcmin in angle. They were accurate enough to make alignment without additional adjustment mechanisms.

The coating at the corners of the grating delaminated slightly after a few thermal cycles between room temperature and liquid helium temperature. This has not become a significant problem, however, because the damaged area has not increased and is not used for diffraction.

3. Measurement

3.A. Measurement Setup

The performance of the flight grating was measured by a Bomem Fourier transform spectrometer Model DA 3.002 located at the Laboratory of Infrared Astrophysics, Institute of Space and Astronautical Science (ISAS). A schematic drawing of the measurement setup is shown in Fig. 5. The test setup was placed in the sample vacuum chamber of the spectrometer. The spectrometer itself introduced an $f/4$ beam, which was reflected by flat mirror M1 to the grating with the given incident angle of $\alpha = 14°$. Mirror M1 was put on a rotatable stage to adjust the incident angle. The grating was mounted on an X–Y stage, and the position was set relative to the incident beam. A slit of the same size as the MIRS was set on an X–Y–Z stage to simulate the incident light of the MIRS design. A pyroelectric detector was used to measure the signal, which was also placed on an X–Y–Z stage behind a slit of the same size to simulate the flight field mirror, and the light falling onto the exit slit was measured. The focus was adjusted by moving the detector in the optical-axis direction (X), whereas the position of the detector was scanned on the stage in the Y and Z directions to measure the wavelength dispersion and the beam pattern in the slit direction. The intensity of the incident light was measured by putting the same detector facing the incident light at the entrance-slit position. A wire-grid polarizer in a rotatable mount was placed in front of the entrance slit in the polarization measurement.

All the measurements were made with a resolution of 2 cm^{-1}. The errors in the diffraction efficiency and

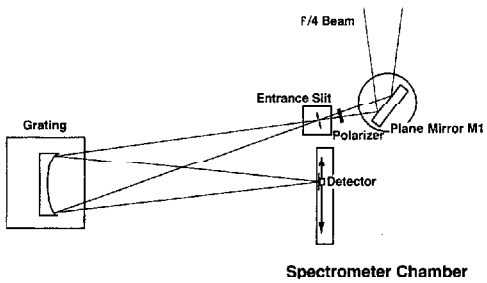

Fig. 5. Schematic diagram of the MIRS grating measurement setup. All the equipment was placed in the spectrometer sample chamber. Flat mirror M1 was placed on a rotatable stage, whereas a slit and a detector were mounted on X–Y–Z stages. The grating was placed on an X–Y stage. A wire-grid polarizer in a rotatable mount is placed in front of the entrance slit. The arrow indicates the movement of the detector for scan in the dispersion direction.

polarization measurement were estimated from the stability of the incident intensity and the rms noise of the baseline. The incident light was shown to be unpolarized within 3%, and thus the polarization characteristics do not affect the results of the diffraction efficiency within the measurement error.

2.B. Results

An example of the measured spectrum is shown in Fig. 6. The first-order (1400-cm^{-1}) and the second-order (2800-cm^{-1}) lines are clearly seen in the figure. The background level shows no excess more than the measurement errors, indicating that the scattered light should be less than 2%. There are no signs of ghost lines. The flight grating behaves basically as a good disperser.

We obtained the wavelength resolution by fitting the observed spectrum by a Gaussian function. It gives a good measure for the FWHM, which is to be compared with $\Delta\lambda$. The Gaussian fit does not fully represent the rapid cutoff of the outer wing in the observed profile but this does not affect the estimation of the FWHM.

Examples of the observed spectra and fitted profiles are plotted in Fig. 7. The FWHM estimated at each wavelength as described above is plotted in Fig. 3 by open circles. As can be seen in Fig. 3, the measured resolution is in good agreement with the predicted resolution. The full width of the spectral line was also measured to be compared with the sum of $\Delta\lambda$ and $\Delta\lambda_g$. Within the measurement errors, the full widths of the spectral lines were the same as twice the FWHM plotted in Fig. 3. The measurement at long wavelengths has relatively large errors partly because the grating efficiency decreases with wavelength (see below and Fig. 10) and partly because the sampling in the wavelength domain becomes sparse for long wavelengths. Because of these errors, the increase of the full width of the spectral line with the wavelength, which was predicted by Eq. (14), was not confirmed in the current measurement. The spectral resolution provided by the flight grating with the designed configuration is shown to be enough to meet the MIRS requirement and have no appreciable degradation caused by the aberration from the grating.

Figure 8 shows the measured central wavelength for various positions of the detector. The position refers to the Y coordinate in Fig. 1. The solid line indicates the expected relationship. The error in the position measurement is approximately 0.1 mm, and the results indicate a good agreement with the ex-

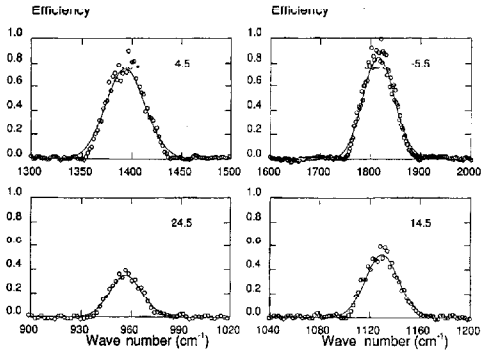

Fig. 7. Examples of the measured spectral line profile (open circles) and the Gaussian fits (solid curve). The detector positions (in millimeters along the Y axis) are indicated in the upper right-hand corner.

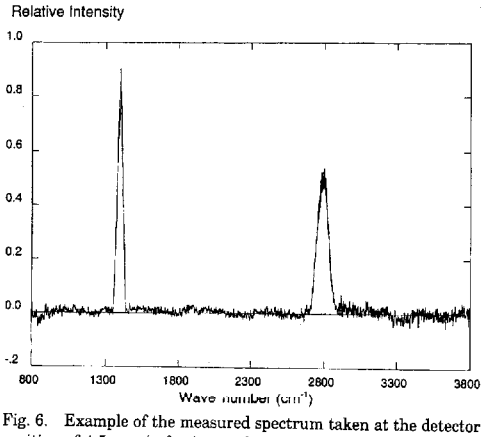

Fig. 6. Example of the measured spectrum taken at the detector position of 4.5 mm (referring to the Y coordinate in Fig. 1). The spectral resolution is 2 cm^{-1}. The ordinate is the relative intensity normalized by the incident intensity. Two peaks are clearly seen: one is the first-order diffraction (~ 1400 cm^{-1}), and the other is the second-order diffraction (~ 2800 cm^{-1}).

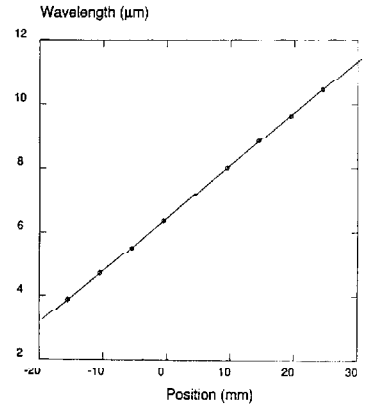

Fig. 8. Position versus wavelength. The position refers to the Y coordinate shown in Fig. 1. The solid line indicates the relationship given by Eq. (5), whereas the open circles show the measured central wavelength of each spectral line. Error bars of the measured wavelengths are in most cases smaller than the symbol.

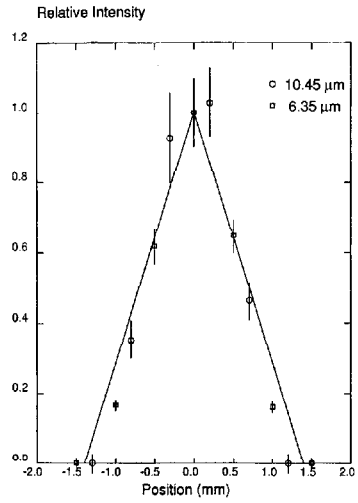

Fig. 9. Beam-pattern profile. The solid line indicates the expected beam pattern, whereas the squares and circles indicate measured patterns at 6.35 and 10.45 μm, respectively. All points are normalized at the peak.

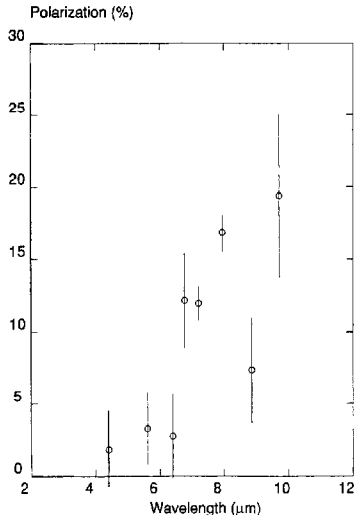

Fig. 11. Polarization of the MIRS grating. The positive polarization is defined as being in the dispersion direction.

pected relationship and good linearity of the wavelength with respect to detector position.

We estimated the spatial beam pattern by moving the detector in the slit direction. The results are shown in Fig. 9, in which the intensities are estimated at the peak of the spectral line profile and normalized at the center position. The measurements were made at two wavelengths (6.35 and 10.45 μm). No definite changes were seen in the central wavelengths and the spectral linewidths with respect to spatial position and there was no difference seen between the beam profiles of the two wavelengths. The expected beam profile is plotted by a solid line in Fig. 9. The measured points agree with the expected profile except in the outer wings. The measured wings are a bit less than the expected extent but not significantly different. The spatial profile was also proved to have the expected characteristics.

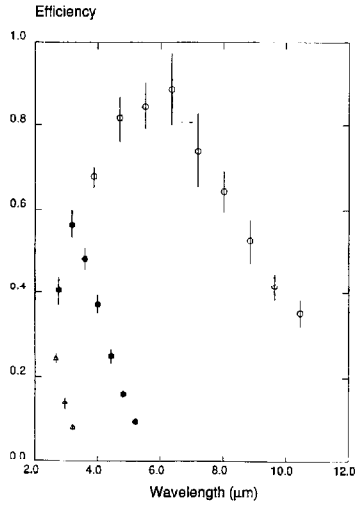

Fig. 10. Measured diffraction efficiency versus wavelength. Open circles indicate the first-order diffraction, and filled circles and open triangles show the second- and third-order diffraction, respectively. The ordinate is normalized by the incident intensity.

The efficiency of the diffraction, which was derived as the peak of the fitted Gaussian, is plotted in Fig. 10. As indicated in Fig. 7, the peak gives a good measure of the efficiency. The efficiencies of the second order and the third order, if measured, are plotted together with the efficiency of the first-order diffraction. The measured first-order efficiency is quite high (>80%) around the blaze wavelength (~6 μm) and decreases gradually for shorter and longer wavelengths. The higher-order diffraction efficiencies follow this trend. The decrease is not unexpected because the wavelength range covers more than one octave. The results show that the efficiency is quite high around the blaze wavelength and stays in the level of more than 30% even at long wavelengths, indicating that the grating has a high enough diffraction efficiency to meet the MIRS requirement.

Finally, the polarization caused by the grating was measured by the placement of a wire-grid polarizer in

front of the entrance slit. Because a high accuracy was needed to obtain the polarization in the differential measurement, the integrated intensity within the FWHM of the line was used to estimate the polarized intensity instead of the peak of the Gaussian profile. The results are plotted in Fig. 11, where the positive polarization is defined as being in the dispersion direction.

For $\lambda < 6.4$ μm, no appreciable polarization more than the measurement errors is detected. Definite polarization of approximately 10% is indicated for λ at 6.7 μm and increases with the wavelength in general, approaching 20% at 9.7 μm. However, the trend is not smooth because a dip is seen at 8.9 μm.

A similar trend in the polarization with the wavelength of a similar amount ($\leq 30\%$) was found in the MIRS performance testing.[1] The current result confirms that a significant fraction of the instrumental polarization of the MIRS comes from the grating.

4. Summary

An aberration-corrected concave grating was designed for the MIRS aboard the IRTS space mission, and the room-temperature performance of the flight grating was tested. The measurements confirmed that the produced grating behaves basically as expected and meets the requirements of the MIRS. The spectral resolution and the beam profile were in good agreement with predictions, whereas the diffraction efficiency was reasonably high over the entire MIRS wavelength range. The grating causes polarization at $\lambda > 6.7$ μm and increases to approximately 20% at 9.7 μm. The results indicate the potential applicability of this kind of grating in future IR instruments, because it enables a compact and simple design with reasonably good spectral and spatial resolution together with a flat focal plane.

The IRTS is a project managed and operated by the ISAS, Japan, in collaboration with NASA. The MIRS has been developed in collaboration between the NASA Ames Research Center and the University of Tokyo. The MIRS grating was made by Hitachi Ltd. The author thanks all the members of the IRTS project, K. Sakai for suggesting the application of this type of grating to the MIRS, T. Kita and T. Harada for useful comments, and T. L. Roellig for efficient collaboration on the MIRS project and reading the manuscript. He is also grateful to the members of the Laboratory of Infrared Astrophysics of ISAS for providing the experimental facility and, in particular, to H. Shibai for helping with the measurements at various stages.

This research was supported in part by a Grant-in-Aid for Scientific Research from the Ministry of Education, Science and Culture of Japan.

References

1. T. L. Roellig, T. Onaka, T. J. McMahon, and T. Tanabe, "The mid-infrared spectrometer on the Infrared Telescope in Space (IRTS) mission," Astrophys. J. **428,** 370–376 (1994).
2. H. Murakami, J. Bock, M. Freund, H. Guo, T. Hirao, A. E. Lange, H. Matsuhara, T. Matsumoto, T. J. McMahon, M. Murakami, T. Nakagawa, M. Noda, K. Noguchi, H. Okuda, K. Okumura, T. Onaka, T. L. Roellig, S. Sato, H. Shibai, T. Tanabe, T. Watabe, T. Yagi, N. Yajima, and M. Yui, "The Infrared Telescope in Space (IRTS)," Astrophys. J. **428,** 354–362 (1994).
3. T. Onaka, T. Yagi, H. Shibai, T. Kohno, T. Tanabe, and H. Murakami, "Optical system of the Infrared Telescope in Space (IRTS)," Appl. Opt. **33,** 1880–1888 (1994).
4. K. J. Wildeman, D. A. Beintema, and P. R. Wesselius, "The Dutch scientific instrument on board IRAS," J. Br. Interplanet. Soc. **30,** 21–26 (1980).
5. M. Wells, S. Chakaveh, R. D. Joseph, A. V. Pattni, M. J. Selby, D. Lemke, P. Lutzow-Wentzky, P. Vaughan, and F. Garzon, "ISOPHOT-S, a low resolution 2.5–12 μm spectrometer for ISO," in *Proceedings of the 22nd Eslab Symposium on Infrared Spectroscopy in Astronomy,* B. H. Kaldeich, ed. (European Space Agency, Noordwijk, 1989), pp. 571–573.
6. M. Noda, T. Matsumoto, S. Matsuura, K. Noguchi, M. Tanaka, and M. A. Lim, "Near-infrared spectrometer on the Infrared Telescope in Space," Astrophys. J. **428,** 363–369 (1994).
7. W. T. Welford, "Aberration theory of gratings and grating mountings," in *Progress in Optics,* E. Wolf, ed. (Pergamon, New York, 1965), Vol. 4, pp. 241–280.
8. T. Harada and T. Kita, "Mechanically ruled aberration-corrected concave gratings," Appl. Opt. **19,** 3987–3993 (1980).
9. H. G. Beutler, "The theory of the concave grating," J. Opt. Soc. Am. **35,** 311–350 (1945).